Available online at www.sciencedirect.com
SCIENCE DIRECT
Catalysis Today 101 (2005) 81–91
CATALYSIS TODAY
www.elsevier.com/locate/cattod

Engineering and chemical aspects of the preparation of microstructured cobalt catalyst for VOC combustion

J. Łojewska [a,*], A. Kołodziej [b], P. Dynarowicz-Łątka [a], A. Wesełucha-Birczyńska [a]

[a] *Faculty of Chemistry, Jagiellonian University, Ul. Ingardena 3, 30060 Krakow, Poland*
[b] *Institute of Chemical Engineering PAS, Bałtycka 5, Pl 44-100 Gliwice, Poland*

Available online 2 March 2005

Abstract

VOC combustion is a demanding process for both reactor and catalyst design. The microstructural reactor made of wire gauze was studied by us as an alternative to ceramic monoliths. The reactor evaluation was based on modeling heat and mass transfer through the selected microstructures. Chromium–aluminum and chromium–nickel steel was surveyed in terms of their applicability for carrier manufacturing and catalyst depositing. The alumina washcoat and cobalt catalyst were deposited as organic precursors using Langmuir–Blodgett (LB) method. The amount of deposited materials was controlled by the LB parameters and verified by TG measurements. The carriers were characterized at various stages of the preparation by SEM/EDX, XPS and RM methods and tested in *n*-hexane combustion. Oxidation of the Al washcoat precursor led to the formation of γ-Al_2O_3 improving the properties of the Al_2O_3 layer (α phase) developed on the precalcined CrAl carrier. Oxidation of cobalt stearate deposited on the CrAl gave dispersed Co_3O_4 spinel. Although the obtained cobalt catalyst in an oxidized state initiated *n*-hexane combustion at higher temperature (370 °C) than an industrial Pt/Al_2O_3 catalyst used as a reference, it had twice as low activation energy (50 kJ/mol).

Keywords: Microstructural reactors; VOC combustion; Cobalt catalyst; Langmuir–Blodgett method

1. Introduction

Every few years new problems add to already a long list of tasks set for the environment protection. During past two decades, one of the priorities – reduction of CO and NO_x emission from vehicle engines – has been successfully solved. Today, removal of volatile organic compounds (VOC) has become a new challenge for chemists, engineers and technologists. That is because catalytic combustion of VOC, still the most promising way to reduce their emission, is in fact an extremely demanding process for both catalysts and converter constructions.

From the chemical point of view, the VOC problems significantly differ from those of CO/NO_x removal. One of the differences is the formation of toxic side products such as dioxins and furans; and another—catalyst deactivation due to the coke formation and sintering. Coke appears as a product of polycondensation of heavy organic molecules, while sintering is a result of the process authothermy. Since, additionally, combustion proceeds in diffusional rather than in kinetic regime, heat and mass transport are determining for the whole process. An optimal solution for VOC removal should thus combine a reactor design in microscopic scale and optimization of a fine catalyst structure.

Classic reactors with dumped beds of catalyst particles are one of the possible solutions for VOC combustion processes. In fact, the reactors with packed beds are easy to construct, but they cause a high-pressure drop and do not allow reducing particle size to obtain high specific surface area. Lacking such drawbacks, monolithic catalytic reactors, and especially ceramic ones [1], have become worldwide standards for catalytic processes of combustion of CO and organic compounds. They, however, have their own limitations such as significant thermal inertia and low heat and mass transfer coefficients between flowing fluid and catalyst surface. These may lead to serious malfunctions especially when confronted with VOCs.

* Corresponding author. Fax: +48 12 6340515.
E-mail address: lojewska@chemia.uj.edu.pl (J. Łojewska).

0920-5861/$ – see front matter © 2005 Elsevier B.V. All rights reserved.
doi:10.1016/j.cattod.2005.01.005

VOC combustion catalysts should most of all secure low temperature of the oxidation initiation as well as the resistance to the coke formation and sintering. An alternative to commonly applied but expensive noble metals seem transition metal oxides [2–5], and in particular, showing high temperature resistance, spinel-, corundum- or perovskite-type oxides [3,6]. Despite their high activity and stability, noble metals cannot overcome the problem of carbonaceous deposits, including particulate matter [5]. However, these used in combination with transition metal oxides can produce flexible catalysts for various kinds of reactions, which may occur during VOC combustion [7–9]. Among oxides, cobalt spinel appears promising for its relatively low temperature of combustion of both VOC oxygenates [3] and sooth particles [10–12].

To overcome at least part of the above listed problems connected with VOC combustion, we propose a structured reactor built of wire gauzes made from chromium–aluminum steel with Co_3O_4/Al_2O_3 catalyst. The application of a metallic microstructure to catalytic reactions requires, however, the development of an efficient method for catalyst layering, which on the one hand, would secure high dispersion and a desired catalyst structure, and would not change the carrier geometry, on the other.

In this work, we tested the Langmuir–Blodgett (LB) technique for washcoat and catalyst layering to obtain γ-Al_2O_3 and Co_3O_4 spinel on the precalcined metallic surfaces. The description of this technique as well as the details on its application can be found elsewhere [13–15]. In all, it secures a continuous control of several physical parameters of layers transferred (molecular packing, lateral pressure, composition and quantity), which are lacking in other depositing techniques (e.g. chemisorption or impregnation). What attracts our interests is that the LB method gives the opportunity to obtain highly ordered, defectless layers of controlled thickness and architecture on the molecular level. This technique has already been successfully utilized in optics and electronics. First attempts to engage the LB method in catalyst preparation to form both catalyst precursors and active catalysts have been reported recently in [16–19]; thus obtained catalysts based on Pd porphyrins were studied in epoxidation reactions [16] and in hydrogen formation [17], other Pd benzylideneacetone complexes—in electroless metal plating [18,19].

This paper presents some engineering aspects of our converter design and the surface chemistry of obtained materials together with the results of catalytic tests in combustion of *n*-hexane used as a test reaction.

2. Engineering approach to catalytic microstructures design

The question arises why the existing solutions of reactors are insufficient for VOC combustion. In ceramic monoliths low mass transfer coefficients combined with a low concentration of hydrocarbons in end-pipe gases lead to a huge mass transport limitation which usually cause an undesirable decrease in conversion. To restore it, the reactor length should be considerably increased. The transport parameters of typical monolithic structures are presented in Table 1. The capillary channels in the monoliths (typically of 0.8–4 mm in diameter) enforce a laminar flow regime in the range of used velocities of flowing media. Molecular diffusion is therefore a predominant mass transport mechanism within a whole channel, which results in low mass transfer coefficients. This is of particular significance for VOC removal, as they are usually highly diluted (even to ppm level) in fast-flowing streams. Moreover, monoliths are particularly sensitive to coking: coke agglomerates cause clogging of small channels and thus may block a gas stream (Fig. 1). Combustion of coke is difficult even at high temperatures, as oxygen can reach the agglomerate only by a molecular diffusion through long capillary channels. For these reasons, active catalytic systems and appropriate structures displaying enhanced transport properties should be developed to avoid or at least limit coke agglomeration.

Table 1
Parameters of typical ceramic monolithic reactors [1]

cpsi	Equivalent channel diameter (m)	Specific surface (m^2/m^3)	Heat capacity ($kJ/(Km^3)$)
25	0.004191	651	640
50	0.002957	917	640
100	0.002159	1339	560
200	0.001529	1898	540
400	0.001168	2709	300
900	0.000796	4311	340

Transport coefficients for a laminar flow are rather poor, but it is well known that they are inversely proportional to the length of a tube. Assuming uniform distribution of velocity, temperature and concentration, the profiles start to develop at the tube inlet, and soon transform, into a parabolic shape typical of a fully developed laminar flow. Until then, transport coefficients are significantly higher in comparison with those of a laminar flow. This phenomenon is a fundamental idea for a microstructure with enhanced transport properties proposed by us.

Our structure is composed of a stack of fine wire gauzes perpendicular to the flow direction (Fig. 1), similar to the reactors applied for the ammonia oxidation or for the Andrussov process. Such a construction, called by us a ‘gauze microstructure’, will be of particular interest for processes requiring high mass and heat transfer. Eyelets of the wire gauze could be modeled by extremely short capillaries where neither velocity nor temperature and concentration profiles can fully develop (Fig. 2). The transport parameters of exemplary gauzes are collected in Table 2. As can be inferred from Tables 1 and 2, the gauzes show higher specific surface area and lower heat capacities than monoliths. A comparison of mass transport coefficients of both structures is presented in Fig. 2 (values taken from

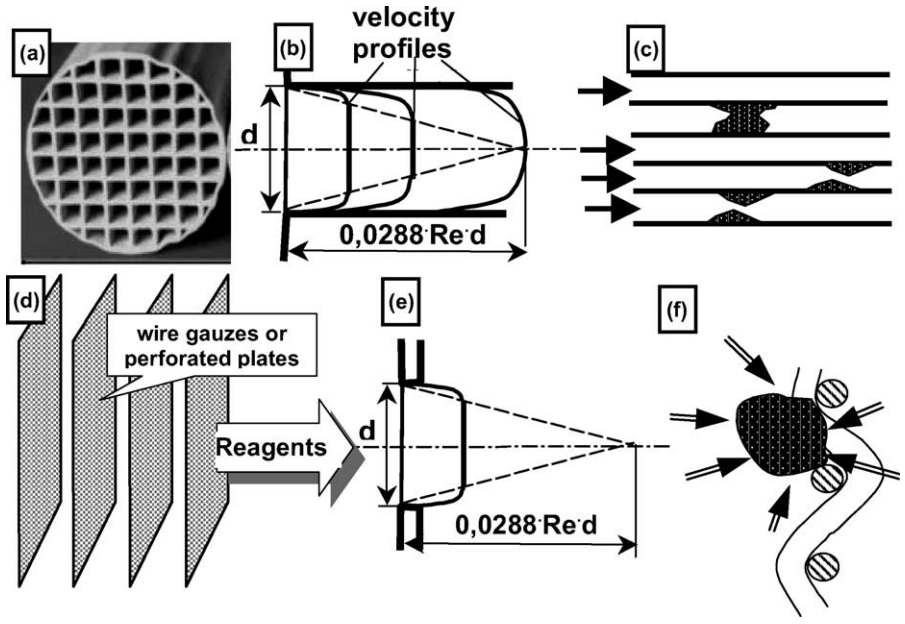

Fig. 1. Comparison of a typical monolithic reactor with a model gauze structure—velocity profiles, coke formation and combustion: (a) ceramic monolith structure, (b) velocity profiles developed in the monolith, (c) clogging by coke agglomerates in the monolith, (d) model gauze structure, (e) partially developed velocity profile in the gauze and (f) combustion of coke agglomerate in the gauze.

Tables 1 and 2). All parameters were calculated using available solutions for transport phenomena occurring during laminar flow [20]. This is noteworthy that for the gauze microstructures the mass transfer coefficients are up to five times higher than for the standard monoliths, while the volumetric mass transfer coefficients are around three times higher.

Another advantage of the gauze microstructure over monoliths can be its resistance to coke, since, as illustrated in Fig. 1, combustion of coke proceeds as long as oxygen can reach an agglomerate from all directions. Thus, at least at the stage of the structure modeling, gauze microstructures seem an excellent tool for VOC catalytic combustion processes.

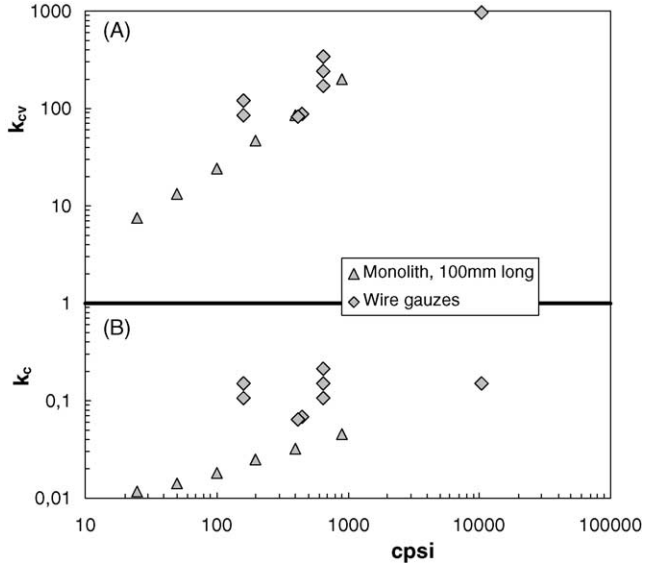

Fig. 2. Comparison of the standard monolith (100 mm) and the wire-gauze microstructure: (A) mass transfer coefficients; (B) volumetric mass transfer coefficients. Case studied of *o*-xylene diffusion in air, 100 °C, and atmospheric pressure. Parameters of monoliths in Table 1, of gauzes in Table 2.

3. Chemistry of the catalytic surfaces

3.1. Experimental

3.1.1. Samples and their nomenclature

Three types of carriers were used for this study: stainless chromium–aluminum steel leaves, denoted as CrAl (00H20J5—0.3 mm thick, Baildon, Poland); chromium–nickel steel woven wire gauze denoted as CrNi (OH18N9—0.2 mm in diameter, Sitodrut, Poland); cobalt foil (99.99+% purity, 0.1 mm thick, Aldrich).

The catalyst preparation consisted of three steps:

Table 2
Parameters of exemplary gauze microstructures

Wire diameter (mm)	cpsi	Equivalent channel diameter (m)	Specific surface (m^2/m^3)	Heat capacity ($kJ/(Km^3)$)
0.1	645.2	0.009	1570	153
0.05	645.2	0.0095	1570	77
0.2	645.2	0.008	1570	307
0.1	161.3	0.019	785	77
0.2	161.3	0.018	785	153
0.5	448	0.007	1308	639
0.55	412.9	0.007	1256	675
0.1	10323	0.0015	6280	614

Table 3
Amounts of Al and Co oxides deposited on carrier samples calculated from LB transfer parameters and from the mass loss of the samples during oxidation of organic groups in TG

Sample name	MeO from LB transfer parameters (nmol/cm^2)	MeO from TG (nmol/cm^2)	Transfer efficiency (%)
Al_2O_3			
Al/CrNi	4.1	1.7	41
Al/CrAl	4.2	3.5	83
Al/Co foil	3.9	3.1	79
Co_3O_4			
1Co/CrAl	10.9	9.7	90
2Co/CrAl	32.7	29.1	89
3Co/CrAl	76.2	70.3	92

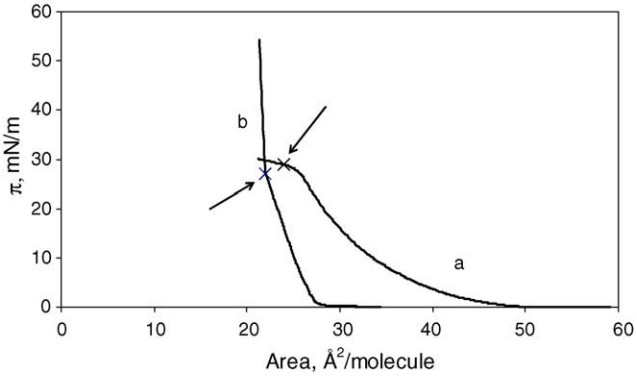

Fig. 3. Isotherms of monolayers composed of: (a) AlR compound and (b) CoSA compound.

(a) precalcination of an initial sample of a carrier in air at 1000 °C for 24 h,
(b) deposition of Al and Co organic compounds on precalcined samples,
(c) oxidation of the deposited samples in TG in a temperature ramp 100–800 °C.

The symbols of the samples undergoing this procedure are included in Table 3.

For depositing, the following compounds were used: for washcoat precursor—aluminum (III) 9-octadecenylacetoacetate diisopropoxide ($C_{28}H_{53}AlO_5$, 90%, Gelest), denoted as AlR; for catalyst precursor—cobalt stearate, $Co(C_{18}H_{35}O_2)_2$, denoted as CoSA. Cobalt stearate was obtained in situ in the Langmuir trough from 0.001 M $Co(NO_3)_2$ aqueous solution (99.999 Aldrich) and stearic acid, SA (99+%, Aldrich) dropped onto $Co(NO_3)_{2aq}$ subphase from chloroform solution (ca. 0.5 g/dm^3).

3.1.2. Catalyst preparation

The metals (Al and Co) composing washcoat and catalyst were deposited from their organic compounds onto the surface of precalcined carriers using the Langmuir–Blodgett method. This was carried out in a single-barrier Langmuir trough (Nima, UK), equipped with a dipping device and a Mini Brewster Angle Microscope (BAM, NFT, Germany). In order to set up the transfer conditions, prior to depositing, isotherms of the monolayers of the selected organic compounds were measured. An isotherm represents a function of surface pressure (π, mN/m) versus surface area occupied by a single molecule in the monolayer (A, Å^2/molecule). To check the material distribution and its homogeneity, the surface was monitored by BAM, which allows for a direct observation of domains and/or phase coexistence at the air–water interface.

The AlR compound was spread from the toluene (Sigma, HPLC) solution (0.24 mg/cm^3) onto bi-distilled water surface from a gas-tight syringe (Hamilton^{TM}). Next, 10 min were allowed for solvent evaporation before the compression was initiated with the speed of 40 cm^2/min. The obtained isotherm of AlR is presented in Fig. 3, curve a. On reaching ca. 28 Å^2/molecule, surface pressure started to increase up to 28 mN/m, when the phase transition began showing a kink on the compression curve. As checked by BAM, the AlR monolayer was homogenous. To avoid a monolayer collapse, the transfer conditions were set up at a starting point of the phase transition: 28 mN/m, 24 Å^2/molecule (indicated by an arrow in Fig. 3, curve a).

Cobalt stearate was prepared from $Co(NO_3)_2$ diluted in bi-distilled water. To secure cobalt stearate precipitation and to stabilise the monolayer, pH of the solution was kept at 5.6 by adding an appropriate amount of HNO_3. Thus prepared solution was poured into a trough chamber. Next, a known volume (0.47 mg/cm^3) of chloroform solution of stearic acid (99+% Aldrich) was spread on the $Co(NO)_3$ solution, and after chloroform evaporation (5 min), the compression began (40 cm^2/min) giving an isotherm presented in Fig. 3, curve b. The phase transition took place at around 22 Å^2/molecule and at surface pressure 27 mN/m. The cobalt stearate precipitation at the air–water interface was monitored with BAM and indicated by changing of the monolayer texture. The transfer conditions for CoSA were set up to: 22 Å^2/molecule and 27 mN/m.

AlR and CoSA compounds were transferred onto all investigated carriers (CrAl, CrNi and Co foil) with the dipping speed of 4 mm/min. After each layer deposition a 5-min time was allowed. The samples were then dried in a desiccator filled with silica gel in air at room temperature for 24 h and were subjected for further analysis.

All in all, 12 monolayers of AlR and 10, 43 and 100 monolayers of CoSA were transferred onto substrates. The expected amount of the deposited material was estimated from the transfer parameters and expressed as Al_2O_3 or Co_3O_4 nmol per geometric area of a carrier (Table 3).

3.1.3. Catalyst characterization

The amount of deposited materials and the transfer efficiency was measured by TG/QMS (Mettler–Toledo). The deposited samples of carriers were oxidized in air until constant mass was achieved, and the amount of remaining Al

and Co oxides was calculated from the loss of sample mass. The oxidation progress was controlled by QMS. Prior to oxidation the samples were conditioned in Ar flowing through the chamber at constant temperatures (50 and 100 °C) to dispose of remaining organic solvents and water adsorbed. Then the inert gas was replaced with air and a temperature ramp 20–800 °C, 10 °C/min was applied.

The samples were investigated at three stages of their preparation (listed above) by several surface techniques: scanning electron microscopy with X-ray microprobe (SEM/EDX), photoelectron spectroscopy (XPS) and Raman microscopy (RM). Due to a low concentration of deposited materials, XRD could not be used to determine the phase composition.

SEM images were obtained in Philips XL 20 microscope equipped with EDX microprobe. XPS analyses were carried out in a VG Scientific ESCA-3 photoelectron spectrometer using Al Kα radiation 1486.6 eV from X-ray source operating at 13 kV and 10 mA. Working pressure was lower than 5×10^{-7} Pa. All spectra were recorded at a photoelectron take-off angle of 45°. Binding energies were corrected to the C 1s peak from the surface carbon at 284.8 eV. The spectra were preprocessed by Shirley's background and Kα band removal. The composite bands were found by fitting single peaks, doublets or multiplets, and finally to find their maxima positions, they were decomposed into symmetric Gaussian–Lorentzian peaks. The spectra were measured in the region of C 1s, O 1s, Mg 1s (for some samples only), Al 2p, Cr 2p, Fe 2p and Co 2p. The measured values of binding energies (BE) are generally in keeping with the reference data found in NIST database. Mole fractions of the elements present on the surface were calculated according to the formula given in [21].

The Raman microspectra (with a resolution 1 cm^{-1}) were collected with a Jobin-Yvon T64000 spectrometer equipped with CCD detector (Spectrum One) using Olympus BX 40 microscope. The sample was excited in backscattering geometry using 514.5 nm line of an Ar^+ ion Spectra-Physics laser (series 2000). Prior to each analysis the surface, under ambient conditions, was examined with an optical microscope at several spots to check the surface homogeneity. The spectra shown in this work correspond to the most typical surface picture of the samples.

3.1.4. Catalytic tests

In the first approach to our kinetic study we used cobalt catalysts deposited on metallic carriers for the oxidation of *n*-hexane performed in a tubular microreactor. A microreactor unit was operated at a continuous flow of reactants at atmospheric pressure. A small glass tube reactor, 4.25 mm i.d., was placed inside a thermostat. A bed filling the reactor was composed of several pieces of a CrAl leaf with the active catalyst deposited. The geometrical surface area of the carrier was approximately 1–2 cm^2 and the height of the bed was around 5 mm.

The reaction mixture contained 20 mol% of O_2, 0.39 mol% of *n*-hexane vapour and the balance of helium. A controlled amount of *n*-hexane vapour was supplied to the reaction mixture from a saturator stabilised at a selected temperature. The *n*-hexane partial pressure at a given temperature was calculated from the Antoine's equation. The reaction proceeded at a total flow rate 103 ml/min and in the temperature range from 100 to 900 °C. The products were analysed using a gas chromatograph (SRI Instruments, 8610C) equipped with TCD detector and the system of two columns packed with Carboxen 1004 and HayesepQ (2 m × 1/16″ in., Supelco).

To obtain temperature dependence of the reaction rate, *n*-hexane oxidation was initiated at 100 °C and after several GC analyses the temperature was increased by 20 °C until CO_2 appeared as a reaction product, since then the temperature was increased by 10 °C and three GC analyses were performed at each temperature. Each point on kinetic curves is a mean value of reaction rate at a given temperature. Beside the temperature dependence, the catalyst stability tests were performed at a temperature of a highest observed conversion.

The reaction rate calculated from GC results was related to the catalyst amount (TOF, 1/s).

3.2. Results and discussion

3.2.1. Quantitative measurements of deposited layers

The amounts of deposited aluminum and cobalt oxides calculated from TG results are presented in Table 3. The values are related to the samples geometric area (both sides). The transfer efficiency is defined as a ratio of the amount of metal oxide measured in TG to that derived from the LB transfer parameters. The least efficiency was observed for the wire gauze sample (41%) whose geometric area available for depositing was twice as low as for the CrAl leaves. For CrAl leaves and Co foil, thus expressed transfer efficiency is greater than the transfer efficiency measured directly in Langmuir trough (amounting to 60%, and measured as a loss of the monolayer area related to a sample geometric area). It has to be taken into account comparing the efficiencies, that the TG results bear rather a high experimental error, since the loss of mass of some samples reached the sensitivity limit of the TG.

The TG results allowed us to elaborate an efficient catalyst activation procedure avoiding long-time high temperature contact of the deposited samples in air to prevent metal oxide sintering. The oxidation of organic parts of the precursors, traced by the loss of the samples mass and the evolution of H_2O and CO_2 lines in the QMS spectrum, is completed after the temperature 800 °C is reached in temperature program 10 °C/min. Further oxidation at 800 °C for another several hours did not give any changes in the monitored properties. Therefore, oxidation in air in temperature ramp 20–800 °C, 10 °C/min, was adapted by us as an activation procedure.

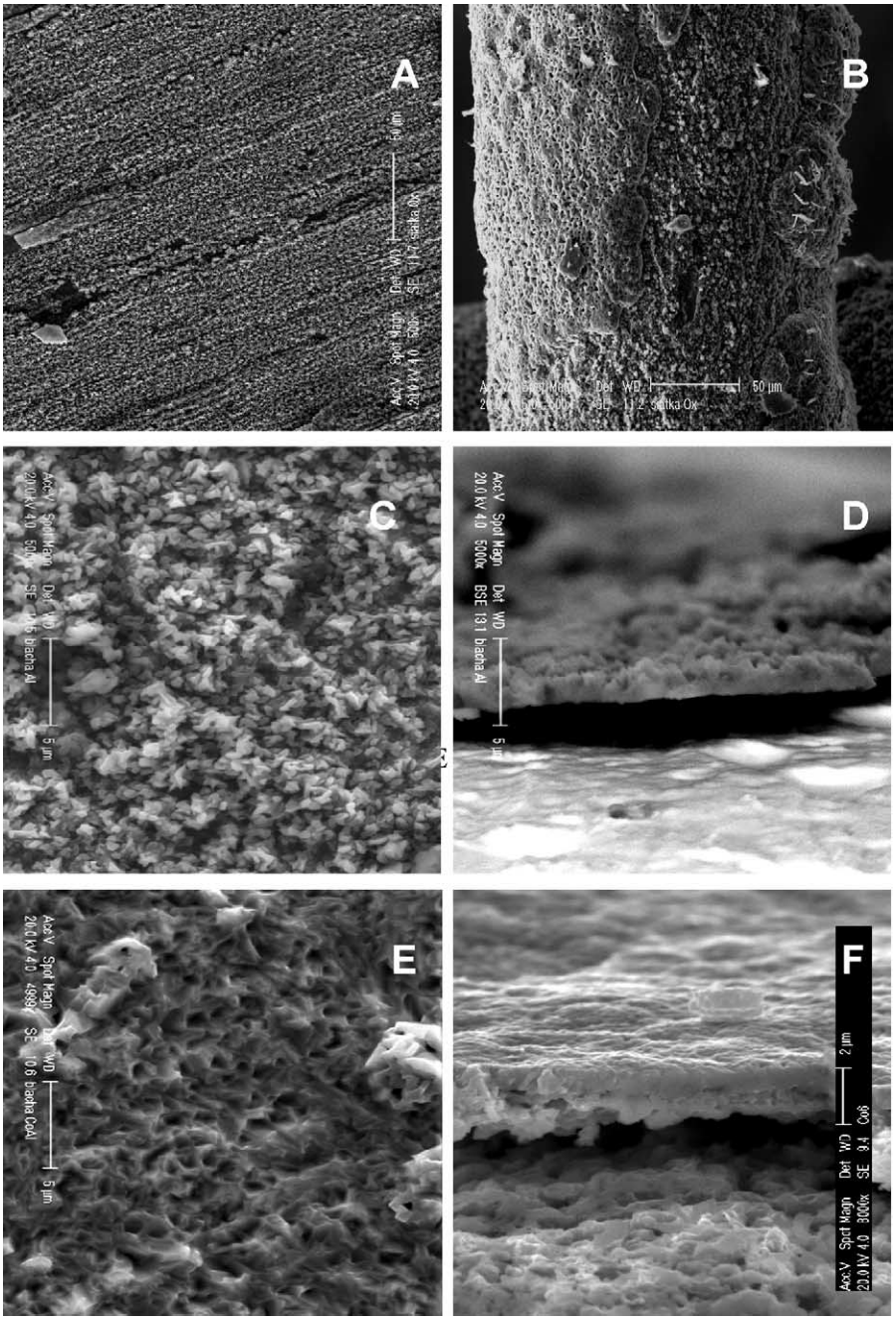

Fig. 4. SEM photographs of the precalcined carriers: (A) surface of CrAl sample (500×); (B) surface of a wire from CrNi sample (500×); (C) surface of CrAl (5000×); (D) a cross-section of the same CrAl sample (5000×); (E) surface of Co sample (5000×); (F) a cross-section of the same Co sample.

3.2.2. Surface analyses

The morphology of the surface of the materials at three stages of the preparation was studied by SEM/EDX. The images of the surface of the initial precalcined samples are presented in Fig. 4. Upon oxidizing at 1000 °C, Al_2O_3 segregates to the surface forming a 2 μm layer built of well-dispersed crystallites less than 1 μm in diameter (Fig. 4A and C). The dimension of the layer is seen in a cross-section of the CrAl leave (Fig. 4D). This layer is rather uniform, however, it shows a directorial texture remained from rolling the steel during leaves manufacturing, and at places where it is thinner, the streaks of iron oxide crystallites can be spotted by back-scattered electrons and EDX. In contrast, the precalcined CrNi steel wire, seen in Fig. 4B, is predominately covered with amorphous iron oxide or mixed iron–chromium oxide layer, but at some places—with Cr, Ni, Fe oxide crystallites, as detected by EDX. Therefore, the CrNi steel appears less suitable as a material for structured carrier especially at an early stage of catalyst modeling. For reference, also the surface of the precalcined sample of Co foil is presented in Fig. 4E together with its cross-section shown in Fig. 4F. The cobalt oxide is less crystalline than

alumina formed on the CrAl. It is worth to point out that a series of subsequent reduction and oxidation at high temperature proved to lead to highly dispersed crystalline cobalt oxide resulting in a high catalytic performance [22,23].

The textures of the deposited and oxidized samples look quite similar to those of the initial samples as observed in images obtained for secondary and back-scattered electrons. Suppose larger crystallites of the deposited alumina and cobalt oxide were formed on contrasting samples (e.g. alumina deposited on the calcined Co foil or cobalt oxide deposited on the CrAl leaves), they should be discernible by back-scattered electrons due to the differences in atomic masses between Al and Co. Because no such effect was observed for our samples, Al and Co oxides must be quite uniformly distributed on the surface of the carriers and do not form aggregates or crystallites discernible in SEM.

XPS analyses were performed in an attempt to assign oxidation states of metals present on the surface, and especially of Co, and to further look into the surface composition of the deposited samples. The binding energies of the studied elements were correlated to specific oxides (Table 4). For the brevity the Mg 1s bands are not included in the tables especially because they were not measured for all the samples. The bands Al 2p, Fe $2p_{(3/2)}$, Co $2p_{(3/2)}$ were assigned to Al_2O_3, FeOHO and CoO, respectively.

The effects of Co and Al deposition can be spotted on contrasting samples, Co on CrAl and Al on CrNi, by the appearance of Co 2p and Al 2p bands in the XPS spectrum. The Co 2p band arising at 781.4 eV was assigned to Co^{2+} and the Al 2p band at 73.8 eV to Al^{3+}. The contribution of the 2p electrons from Co^{3+} to the observed Co 2p band is rather low, if any, on the deposited and the oxidized Co/CrAl samples. Additionally, after CoSA depositing, the shift of Al 2p band towards lower energies, from 74.8 to 74.1 eV was observed. This can be accounted for by the disappearance of OH groups from Al_2O_3 surface, upon ionic exchange with Co^{2+} cations taking place on acidic centers. Apparently, such an exchange does not occur during AlR deposition. Almost total absence of Co_3O_4 on the Co/CrAl samples can be somewhat surprising because Co_3O_4 spinel is more thermodynamically stable under ambient conditions than CoO and transforms to CoO at above 900 °C. Due to the reductive properties of vacuum, Co_3O_4 was found to be able to desorb oxygen and to reduce into CoO at much lower temperatures comparing with those found for classic thermodynamic data [24].

As regards Fe region, the shape of a Fe 2p line, fitted with appropriate multiplets, suggests the presence of iron at +3 oxidation state in the form of mixed hydroxide FeOHO rather than Fe_2O_3. As regards Cr 2p bands on the CrAl samples, the observed values of BE exceed the typical Cr 2p range, from metallic Cr to Cr^{6+} cations. The more detailed investigation of the O 1s region may shed some light on the observed inconsistency regarding Cr 2p range. Oxygen band is complex for all studied samples. For the CrAl samples, it

Table 4
Types of oxides assigned from the values of binding energies (BE) from XPS for carriers at various stages of preparation

Sample name	Band	Oxide type	Preparation stage (BE, eV)		
			Precalcined	Deposited	Oxidized
Al/CrAl	O 1s	Fe_2O_3[a]	529.6	530.0	530.0
		Al_2O_3	530.9	531.3	531.1
		H_2O/Cr_2O_3	532.4	532.9	532.6
		C–O	–	534.3	–
	Al 2p	Al_2O	73.8	74.0	73.9
	Cr 2p	–	Low intensity	Low intensity	Low intensity
	Fe $2p_{(3/2)}$[b]	–	Low intensity	Low intensity	Low intensity
2Co/CrAl	O 1s	CoO	–	–	529.3
		Al_2O_3	531.0	531.3	531.2
		H_2O/Cr_2O_3	533.0	533.2	533.1
	Al 2p	Al_2O_3	74.8	74.1	74.1
	Cr 2p	Cr	–	572.3	–
		Cr_2O_3[c]	577.2	577.3	577.2
		CrO_4^{2-}	581.4	580.9	582
	Fe $2p_{(3/2)}$	FeOHO	711.3	711.4	711.3
	Co $2p_{(3/2)}$	CoO	–	781.4	781.2
Al/CrNi	O 1s	Fe_2O_3	529.8	529.8	529.8
		H_2O	531.7	531.5	531.6
		Cr_2O_3	533.0	532.8	533.0
	Al 2p	–	–	73.8	74.0
	Cr 2p	Cr_2O_3	576.3	576.4	576.4
	Fe $2p_{(3/2)}$	–	Low intensity	Low intensity	Low intensity

[a] Optional fitting not included in further analyses.
[b] Intensity of this band was too low for reasonable BE assignment.
[c] Most reliable band assignment for a main intensity.

is composed of a symmetric peak coming from aluminum oxide (BE = 530.9 eV), accompanied by a small satellite of a higher energy, which can be assigned to oxygen in OH or in chromium (III) oxide. Fitting another satellite, the 3rd lower energy peak with a maximum at 529.6 eV typical of iron (III) oxide found for the initial CrAl sample, is more a question of our knowledge of the surface composition than a result of a better optimization. We showed this band as an option for the precalcined CrAl sample. Upon depositing all O 1s bands shifted by around 0.4 eV towards higher energies and a new small band attributed to carbon–oxygen bonding (as in carboxylic groups or carbonyl groups) appeared at 534.3 eV. Further oxidation brought about a shift of O 1s in H_2O/Cr_2O_3 region towards slightly lower energies, which is accompanied, by the shift of Cr 2p band (see Co/CrAl sample). A possible explanation of the observed effects can be either the chemical environment modification of the atoms present on the surface, or the change in electron conductivity (surface charging) caused by shielding the surface with the metal organic compounds or metal oxides. This might have given rise to the change in the work function giving a lower value of electron kinetic energy. The fact that other studied lines of the CrAl samples: Al 2p, Fe $2p_{(3/2)}$, were less prone to such changes upon the samples treatment may give a hint as to the sequence of metal oxides occurring in the surface region of the CrAl samples. Following this train of thought, the CoSA on the CrAl, which oxidizes into cobalt oxide, covers surface chromium species and not iron oxide. The same may concern Al deposited on the CrAl, but the Cr 2p lines this time were too weak for the reliable conclusions.

The surface composition of the studied materials based on XPS results is presented in Tables 5 and 6. In Table 5 various carriers are compared. Table 6 relates a series of differently loaded Co catalyst deposited on the CrAl carrier. The concentrations of all elements found from the band intensities, for the sake of the paper conciseness, were recalculated to the molar fractions of oxides found above:

Table 5
Composition of surface region of carriers calculated from XPS

Carrier sample	MeO	MeO molar fraction at a given preparation stage	
		Precalcined	Deposited/oxidized
Al/CrAl	Al_2O_3	0.613	0.620
	Cr_2O_3	0.028	0.045
	FeOHO	0.048	0.033
	Other OHs	0.312	0.302
2Co/CrAl	Al_2O_3	0.678	0.673
	Cr_2O_3	0.038	0.065
	FeOHO	0.120	0.111
	CoO	–	0.018
	Other OHs	0.165	0.134
Al/CrNi	Al_2O_3	–	0.083
	Cr_2O_3	0.333	0.323
	FeOHO	0.159	0.138
	Other OHs	0.509	0.457

Table 6
Surface concentration of Co oxide deposited on the CrAl leaves calculated from XPS

Sample name	Surface composition from XPS (mole fractions)			
	CoO	Al_2O_3	Fe_2O_3	Cr_2O_3
1Co/CrAl	0.006	0.253	0.018	0.017
2Co/CrAl	0.016	0.233	0.032	0.023
3Co/CrAl	0.004	0.293	0.021	0.021

Al_2O_3, Cr_2O_3, FeOHO and CoO. The remaining oxygen was attributed to H_2O or OH present on the surface (O 1s, BE = 533 eV), and denoted as 'other OHs'. As seen in Table 5, the prevailing compounds are Al_2O_3 on the CrAl samples and Cr_2O_3 on the CrNi gauze. A relatively high contribution of OHs in the surface region is due to a large amount of Mg detected on the CrAl samples (Mg molar fraction is on average 0.05). It also seems interesting to note that the amount OH is greater for the precalcined CrAl used for Al deposition that was kept in a desiccator under dehydrating conditions for a shorter time, than for the precalcined CrAl used for Co deposition. This may also explain why the intensities of Cr 2p and Fe $2p_{(3/2)}$ were much lower for this sample. Apparently, dry conditions favor iron and chromium oxides segregation to the surface. The interpretation of the CrNi sample is more difficult since it is not uniform. Comparing the series of Co catalyst presented in Table 6, the lowest amount of CoO was detected on the surface of the most loaded 3Co/CrAl sample. Taking into account that photoelectrons come from a very superficial region of the sample this result implies reduced dispersion of cobalt oxide on this sample.

From the XPS perspective, deposited metals do not cover the surface uniformly, as a monolayer, and form some sort of aggregates, which are not large enough to be spotted in SEM. If there were opposite, a molar fraction of a deposited compound should reach the value of 1.

Raman micrographs give another perspective to our understanding of the material structure because RM is less a surface technique than both SEM and XPS. The dimension of the surface region available for the light is large, although in practice immeasurable. The initial precalcined CrAl samples show small but sharp bands at 380 and 410 cm^{-1} and broad bands at 521, 634 and 721 cm^{-1} (Fig. 5A, curve a). The alumina layer formed on the sample has a small contribution of crystalline phases resembling that of α-Al_2O_3 (corundum structure) [25]. Pure dispersed γ-Al_2O_3 metaphase, highly demanded for catalytic applications, does not give any Raman signal in the studied range of wavenumbers, as measured by Jongsomjit et al. [26,27]. Upon depositing AlR compound onto the CrAl carrier, a sharp peak appears at 410 cm^{-1} and less intense at 372 cm^{-1} (Fig. 5A, curve b), which is characteristic of Al–O stretching vibrations [28]. Further oxidation of AlR gives rise to the disappearance of the former α-Al_2O_3 and the formation of dispersed Al_2O_3, probably of a γ type, at least in the subsurface region available for Raman scattering. A

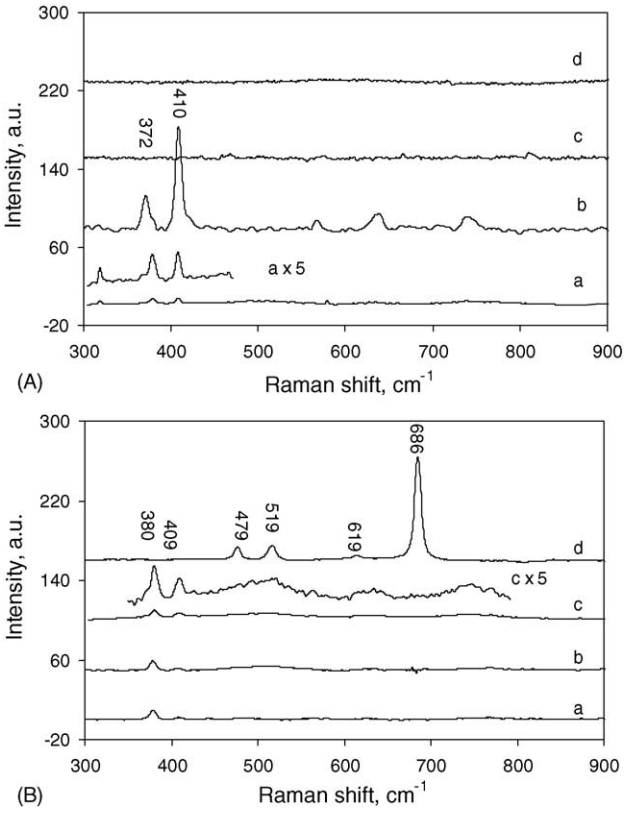

Fig. 5. Raman spectra of the samples at various stages of the treatment—(A): Al/CrAl sample (curve a) precalcined with a spectrum multiplied by 5 (curve a × 5), (curve b) deposited with AlR, (curve c) 'b' oxidized in temperature ramp 100–800 °C and (curve d) reference sample of Al_2O_3 obtained from AlR oxidized in temperature ramp 100–800 °C; (B): 2Co/CrAl sample (curve a) precalcined, (curve b) deposited with CoSA, (curve c) 'b' oxidized in temperature ramp from 100 to 800 °C and (curve d) reference sample of precalcined Co foil.

reference spectrum of the alumina obtained by a direct oxidation of AlR complies with the latter spectrum of the alumina deposited on the CrAl (compare curve, c and d in Fig. 5A).

As regards Co deposition, the Raman micrographs presented in Fig. 5B suggest the presence of Co_3O_4 rather than CoO. On the precalcined Co foil, used as a reference sample (Fig. 5B, curve d), the bands 686, 619, 519 and 479 are characteristic of Co_3O_4 spinel [27]. According to the cited paper, the Co_3O_4 spectra do not differ from the CoO spectra, whatsoever, implying that both of them must have come from the same oxide. This evidences clearly that at ambient conditions CoO oxidizes to Co_3O_4. The CrAl sample deposited with CoSA and then oxidized at 800 °C shows, except the original modes from α-Al_2O_3, three fairly broad bands at around 750, 630 and 520 cm^{-1} (Fig. 5B, curve c), which are slightly different than those of a pure spinel. It must be stressed though, that positions of Raman signals of vibrational modes are sensitive to the chemical environment and may vary even within 50 cm^{-1} [29]. Other broad bands found for the Co/γ-Al_2O_3 catalyst at 560 and 690 cm^{-1}, were correlated to the so-called highly dispersed

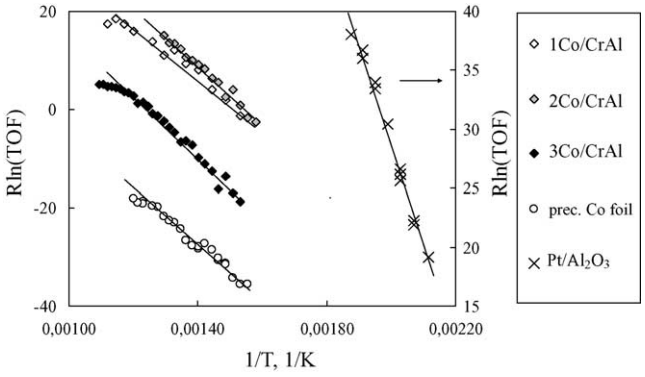

Fig. 6. Arrhenius plots of various Co catalyst used for combustion of *n*-hexane compared to the industrial Pt/Al_2O_3 catalyst.

cobalt 'aluminate' phase [30], which can be understood in terms of catalyst–support strong interactions occurring especially when metal oxide is highly dispersed. Therefore the cobalt oxide formed on the precalcined CrAl could be attributed to highly dispersed spinel. The formation of the $CoAl_2O_4$ spinel structure can be definitely excluded comparing the spectra from Ref. [30]. Let us note that, as reported in Ref. [31], the Raman spectra of cobalt catalyst on Al_2O_3 of much higher cobalt oxide amount than used in our samples, can be situated somewhere between pure Co_3O_4 spinel spectrum and the spectrum of the Co_3O_4 dispersed on the CrAl surface.

3.2.3. Catalytic tests

The results of the kinetic tests of a series the cobalt catalysts of various loading (1Co/CrAl, 2Co/CrAl, 3Co/CrAl) and of the reference samples (precalcined Co foil and commercial Pt/Al_2O_3 catalyst) are presented as Arrhenius plots in Fig. 6 and Table 7. These were prepared according to the following kinetic approach. Oxidation of *n*-hexane (C6) can be expressed by the overall stoichiometric equation:

$$C_6H_{12} + 6O_2 \rightarrow 6CO_2 + 6H_2O \quad (1)$$

However, in the oxygen excess (oxygen concentration, CO_2 constant) can be simplified into a simple reaction pattern described by a simple first-order kinetic equation:

$$r = kC_{C6} = A_{app} \exp\left(\frac{-E_{A,app}}{RT}\right) C_{C6} \quad (2)$$

Table 7
Kinetic parameters derived from fitting Arrhenius equation to the kinetic curves of *n*-hexane combustion

Sample name	Temperatue range[a] (°C)	A_{app} (1/s)	E_{app} (kJ/mol)
1Co/CrAl	420–600	2.4×10^3	46
2Co/CrAl	360–500	8.4×10^4	54
3Co/CrAl	350–740	1.6×10^4	57
Co foil	350–570	2.2×10^2	52
Pt/Al_2O_3	210–260	5.3×10^8	86

[a] Temperature range in which the reaction rate behaves according to Arrhenius equation.

where r is a reaction rate, k the rate constant, C_{C6} the n-hexane concentration in the gas phase, A_{app} the pre-exponential factor and E_{app} the activation energy. If the number of active centres is known, the specific reaction rate can be defined as turnover frequency (TOF, 1/s). Note that for the low surface concentration of the highly dispersed catalyst (which is the case of our Co_3O_4 catalyst), the number of active centres can be approximated to the catalyst amount. Finally, approximating the test reactor to a plug flow differential reactor (C_{C6} approximately constant), the kinetic equation can be simplified:

$$r\,(1/\mathrm{s}) \cong A_{\mathrm{app}} \exp\left(\frac{-E_{\mathrm{A,app}}}{RT}\right) \quad (3)$$

which is the expression used to obtain Arrhenius plots presented in Fig. 6. According to the differential reactor assumption, the reaction rate was calculated directly from C6 conversion.

In the used reactor and under the conditions applied, the superficial velocity of a gas amounts to 0.12 m/s and Reynolds number defined for the hydrodynamic diameter is 2.4 (for an empty reactor tube diameter $Re = 7.8$). The media flow is therefore evidently laminar, which inevitably places the reaction in a diffusional regime, especially at higher temperatures. Since the calculated reaction rate and kinetic parameters do not reflect intrinsic catalytic reaction and are combined with diffusional effects, the derived parameters are apparent and must be treated more qualitatively than quantitatively. Additionally, the assumption of a differential reactor allowing calculating the reaction rate from C6 conversion is weaker at higher temperatures (500 °C) when the conversion reaches 40% (a maximum conversion observed under the applied reaction conditions). Nonetheless, the apparent kinetics can be used for a rough evaluation of the catalytic performance and the methods of catalyst preparation as it is shown below.

To comprehensively describe the catalysts performance the catalyst activity should be regarded in terms of not only reaction rate (or conversion) at a certain temperature, but also activation energy and the catalyst ability to initiate the reaction at a low temperature.

All cobalt catalyst prepared by LB deposition and the reference sample of precalcined Co foil show a common trend on the Arrhenius plot (Fig. 6), with a similar apparent activation energy value amounting to around 50 kJ/mol (Table 7). The pre-exponential factors differ from one another but their interpretation is rather difficult due to an unknown diffusional impact on the reaction rate. All the cobalt catalyst initiated the reaction at around 370 °C, however, the Arrhenius equation was fitted in the temperature range where the results showed linearity (ranges specified in Table 7). In order to discuss the results obtained for cobalt catalysts in a broader context, the reaction was also performed on standard platinum supported catalyst, 0.35 wt.% Pt/Al_2O_3, of a loading similar to the 2Co/CrAl sample. The platinum catalyst showed the highest activity among the studied catalysts, and the lowest initiation temperature (170 °C). The value of the activation energy for platinum catalyst (90 kJ/mol) was almost twice as high as for the cobalt catalysts, which may be a result of a different oxidation mechanism on Pt and cobalt oxide catalysts. Additionally, since Pt catalyst was used as a powder, the result may also indicate strong diffusional limitation for the catalyst on metallic carriers.

In an attempt to exclude possible catalytic effects coming from the oxide matrix of the initial precalcined CrAl sample, we carried out similar n-hexane combustion experiment but with the precalcined CrAl sample in the reactor. This CrAl sample initiated the oxidation at much higher temperature (750 °C) than Co/CrAl catalysts, with the apparent activation energy 390 kJ/mol, giving small amounts of CO_2, CO and an unknown product of n-hexane partial oxidation. The total oxidation with 100% conversion was achieved at 900 °C and most evidently proceeded via noncatalytic homogenous path.

Finally, the time on stream tests performed at 500 °C for 2 h for the Co/CrAl catalyst showed a slight deactivation (4% drop in conversion) most evidently due to the cobalt oxide sintering. For other cobalt catalyst sintering has been proved to initiate as low as at 400 °C [22,23].

4. Conclusions

- The Langmuir–Blodgett depositing method proved suitable to obtain an active catalyst—highly dispersed Co_3O_4 spinel on the Al_2O_3 matrix on the precalcined chromium–aluminum steel. It also allowed controlling the amount of the deposited material. The applied surface techniques (SEM/EDX, XPS, RM) unlike XRD occurred sensitive enough for the detection of the small amounts of the deposited species.
- The conditions of the activation of washcoat and catalyst precursors were elaborated using TG/QMS method. Oxidation of the Al-containing organic washcoat precursor, deposited on the precalcined chromium–aluminum steel, led to the formation of γ-Al_2O_3 metaphase and improved the properties of the Al_2O_3 layer composed partly of α phase. Oxidation of Co stearate catalyst precursor gave a dispersed Co_3O_4 spinel. No organic ligands were found on the surface after the activation procedure was completed.
- The obtained cobalt catalyst tested in combustion of n-hexane occurred relatively active as compared to the Pt/Al_2O_3. Although it initiated the reaction at higher temperature (370 °C), it had almost twice as low activation energy (50 kJ/mol). The maximum n-hexane conversion was estimated to 40%. The derived kinetic parameters are apparent due to strong diffusional limitation of the reaction rate. Thus for further studies targeted at modeling the reaction kinetics gradientless reactor should be applied.

Acknowledgement

This study was supported by the grant from Polish State Committee for Scientific Research (No. 3T09C04627).

References

[1] J.L. Williams, Catal. Today 69 (2001) 3–9.
[2] P.O. Larsson, H. Berggren, A. Andersson, O. Augustsson, Catal. Today 35 (1997) 137–144.
[3] G. Busca, M. Daturi, E. Finocchio, V. Lorenzelli, G. Ramis, R.J. Willey, Catal. Today 33 (1997) 239–249.
[4] M. Ferrandon, M. Berg, E. Björnbom, Catal. Today 53 (1999) 647–659.
[5] A.F. Ahlström-Silversand, C.U.I. Odenbrand, Chem. Eng. J. 73 (1999) 205–216.
[6] L. Marchetti, L. Forni, Appl. Catal. B: Environ. 15 (1998) 179–187.
[7] M. Skonglundh, H. Johansson, L. Löwendahl, K. Jansson, L. Dahl, B. Hirschauer, Appl. Catal. B: Environ. 7 (1996) 299–319.
[8] H. Widjaja, K. Sekizawa, K. Eguchi, H. Arai, Catal. Today 47 (1999) 95–101.
[9] S. Minicò, S. Scirè, C. Crisafulli, R. Maggiore, S. Galvagno, Appl. Catal. B: Environ. 28 (2000) 245–251.
[10] P.A. Neeft, M. Makkee, J.A. Moulijn, Appl. Catal. B: Environ. 8 (1996) 57–78.
[11] J.P.A. Neeft, O.P.P. van Pruissen, M. Makkee, J.A. Moulijn, Appl. Catal. B: Environ. 12 (1997) 21–31.
[12] P.G. Harrison, I.K. Ball, W. Daniell, P. Lukinskas, M. Céspedes, E.E. Miró, M.A. Ulla, Chem. Eng. J. 95 (2003) 47–55.
[13] G.L. Gaines Jr., Insoluble Monolayers at Liquid–Gas Interfaces, Interscience, New York, 1966.
[14] G.G. Roberts, in: G. Roberts (Ed.), Langmuir–Blodgett Films, Plenum Press, New York, 1990, , Chapter 1.
[15] J. Łojewska, P. Dynarowicz Łątka, Z. Piwowarska, A. Kołodziej, Langmuir film deposition as a method of preparation of fine catalyst structure on metallic carriers. Alumina layering on stainless steel surfaces, Langmuir, submitted for publication.
[16] D. Abatti, M. Elisabete, D. Zaniquelli, Y. Iamamoto, I.M. Idemori, Thin Solid Films 310 (1997) 296–302.
[17] D.J. Qian, T. Wakayama, C. Nakamura, J. Miyake, J. Phys. Chem. 107 (15) (2003) 3332–3335.
[18] E. Maassen, B. Tieke, Langmuir 12 (1996) 5601–5605.
[19] T. Beyerlein, F. Bent, B. Tieke, Mater. Sci. Eng. C 8/9 (1999) 93–97.
[20] R.K. Shah, A.L. London, Laminar Flow Forced Convection in Ducts, Academic Press, New York, 1978.
[21] M. Wojciechowska, J. Haber, S. Łomnicki, J. Stoch, J. Mol. Catal. A: Chem. 141 (1999) 155–170.
[22] J. Łojewska, R. Dziembaj, J. Mol. Catal. A: Chem. 122 (1997) 1–11.
[23] J. Łojewska, W. Makowski, T. Tyszewski, R. Dziembaj, Catal. Today 69 (2001) 409–418.
[24] A. Jnioui, M. Alnot, J. Lambert, H. Amariglio, J. Catal. 106 (1987) 144–165.
[25] Spectra online: http://spectra.galactic.com/SpectraOnline, from Galactic Spectral Server.
[26] B. Jongsomjit, J.G. Goodwin Jr., Catal. Today 77 (2002) 191–204.
[27] B. Jongsomjit, J. Panpranot, J.G. Goodwin Jr., J. Catal. 215 (2003) 66–77.
[28] K. Nakamoto, Infrared Spectra of Inorganic Coordination Compounds, Wiley, 1963.
[29] D.R. Clarke, Curr. Opin. Solid State Mater. Sci. 6 (2002) 237–244.
[30] B. Jongsomjit, J. Panpranot, J.G. Goodwin Jr., J. Catal. 204 (2001) 98–106.
[31] T. Xiao, S. Ji, H. Wang, K.S. Coleman, M.L.H. Green, J. Mol. Catal. A: Chem. 175 (2001) 111–123.